Adsorption 11: 415–420, 2005

Adsorption Dynamics of Air on Zeolite 13X and CMS Beds for Separation and Purification

JEONG-GEUN JEE AND SANG-JIN LEE
Department of Chemical Engineering, Yonsei University, 134 Shinchon-dong, Seodaemun-gu, Seoul, 120-749, Korea

HEUNG-MAN MOON
Cryogenic Research Center, Dae-Sung Industrial Gases Co., 781-1 Wonsi-dong, Ansan-si, Gyeonggi-do, 425-090, Korea

CHANG-HA LEE*
Department of Chemical Engineering, Yonsei University,134 Shinchon-dong, Seodaemun-gu, Seoul, 120-749, Korea
leech@yousei.ac.kr

Abstract. The adsorption dynamics of N_2, O_2, and Ar in kinetic separation bed with CMS and equilibrium separation bed with zeolite 13X were investigated by using dried air as a feed. In the CMS bed initially saturated with He, Ar was the first breakthrough component showing a small roll-up and N_2 followed at a very close interval. Then, the breakthrough of O_2 occurred with a broad roll-up due to its fast diffusion rate and the relatively slow diffusion rate of N_2. In the zeolite 13X bed initially saturated with O_2, the breakthrough of Ar first occurred with roll-up owing to the strong adsorption of N_2, then the breakthrough of N_2 followed after a very short interval. Based upon these results, the cyclic adsorption dynamics of the zeolite 13X VSA for air bulk separation and CMS PSA for oxygen purification were studied. The five-step two-bed O_2 VSA with zeolite 13X produced O_2 of over 90% purity with high recovery. The MTZ variation of N_2 during the adsorption and vacuum steps was described in detail. In the case of the six-step two-bed PSA process for O_2 purification, O_2 of 99.8+% purity could be produced from the binary mixture (O_2/Ar—95:5 vol.%). The dynamic adsorption behaviors were investigated by using a concentration-dependent rate model incorporated with mass, energy, and momentum balances. The model reasonably predicted the adsorption dynamics at the equilibrium and kinetic separation beds.

Keywords: separation and purification, adsorption dynamics, zeolite 13X, CMS, air

1. Introduction

The commercial applications for the adsorptive generation of oxygen from ambient air using several zeolites have been grossed during the last 30 years. Especially, the vacuum swing adsorption (VSA) process for air separation is competitive with the pressure swing adsorption (PSA) process for the production of over 15 TPDc oxygen (Yang, 1987). Lots of VSA processes for air separation have generally been operated in the range of 1.1 to 1.8 atm for adsorption pressure and 0.05 to 0.3 atm for desorption pressure. Commercial VSA processes can produce O_2 of 90–94% purity from air.

*To whom correspondence should be addressed.

Recently, the demand for the high purity oxygen of over 99% has increased tremendously in many industries (Hayashi et al., 1996). In addition, the demand for high purity O_2 of over 99.8% is increasing greatly because the semi-conductor industries have been expanded. This high purity oxygen can be produced by removing N_2 and Ar impurities contained in the product of the VSA process. Carbon molecular sieve (CMS) can be used to remove the argon and nitrogen impurities contained in the oxygen-rich gas produced from the VSA process because of its kinetic selectivity between O_2 and other impurities. Therefore, in order to reduce both the energy and equipment cost and to maximize the process performance, it is necessary to understand the adsorption dynamics of air in zeolite 13X bed for air separation and CMS bed for oxygen purification.

To produce high purity oxygen from air, zeolite 13X VSA process as a bulk separator and CMS PSA process as a purifier were studied separately. The adsorption dynamics of air in the zeolite 13X bed and CMS bed were compared by the breakthrough experiments. The VSA process was studied from a viewpoint of cyclic performances such as O_2 purity and recovery. Moreover, the PSA process for removing N_2 and Ar impurities from O_2 enriched feed was experimented.

2. Mathematical Model

The governing equations including mass, energy, and momentum balances, presented in the previous study (Jee et al., 2002; Kim et al., 2004), were applied to VSA and PSA processes. The multi-component adsorption equilibrium was predicted by the LRC model.

The common LDF model assuming constant diffusivity was applied to the zeolite 13X bed while the modified LDF model with following concentration-dependent diffusivity was applied to the CMS bed.

2.1. *Gluekauf's LDF Model for Zeolite 13X*

$$\frac{\partial \overline{q_i}}{\partial t} = \omega_i(q_i^* - \overline{q_i}), \quad \omega_i = \frac{KD_{ei}}{r_c^2} \tag{1}$$

In this model, the effective diffusivity, D_{ei}, was assumed constant. Because the diffusion time constants of O_2, N_2 and Ar on zeolite 13X showed little concentration dependency, this model was used in the equilibrium bed.

2.2. *Modified LDF Model for CMS*

The following structural diffusion model (Do, 1996) represents the strong concentration dependency of diffusional time constant, D_{ei}/R_p^2.

$$D_{ei} \approx \frac{D_{oi}}{dq_i/dP_i} \tag{2}$$

Recently, Bae and Lee (2004) suggested a modified structural diffusion model by using a supercritical relationship. The modified model with the Langmuir isotherm can be presented as follows:

$$\frac{\partial \overline{q_i}}{\partial t} = \omega_i(q_i^* - \overline{q_i}), \quad \omega_i = \frac{KD_{ei}}{R_p^2} \tag{3}$$

where $\frac{D_{ei}}{R_p^2} = C \cdot P_r^{0.5}(1 + B_i P_i)^2$

3. Experimental Section

In the breakthrough and VSA experiments, the adsorption bed was made of stainless-steel pipe with a length of 100 cm, an ID of 3.44 cm, and a wall thickness of 2.67 mm while in the PSA experiments, the bed used was with a length of 100 cm, and an ID of 2.2 cm, and a wall thickness of 1.75 mm. The flow rate was controlled by a mass flow controller and the total amount of feed flow was measured by a wet gas meter. In order to keep the pressure in the adsorption bed constant, a back pressure regulator was installed between the adsorption bed and the product bed. The experimental bed pressure was measured by pressure transducers equipped at the top and bottom of each bed. The concentration of the influent and effluent was analyzed by a mass spectrometer (Balzers, QMG 422). This analyzer was confirmed by a gas chromatography (HP, 5890II). The system was fully automated by a personal computer with a developed control program, and all the measurements including the flow rate, pressure, temperature, and concentration were saved on the computer through an AD converter. The high performance vacuum pump (Ulvac, DAH-60) was used for a vacuum step of VSA process in the range of 0.2 to 0.4 atm.

As an initial condition, the breakthrough experiments were conducted at the bed saturated by O_2 (99.9+%) for CMS bed and He (99.99+%) for zeolite 13X bed under the same adsorption pressure. The temperatures of the feed, bed, and surroundings were kept in the range of 297 K to 300 K as an initial experimental temperature.

Table 1. Characteristics of adsorbents and adsorption beds.

Adsorbent	Zeolite 13X	CMS
Type	Sphere	Pellet
Average pellet size, R_p [cm]	0.105	0.283
Pellet density, ρ_p [g/cm^3]	0.93	0.90
Heat capacity, C_{ps} [cal/g·K]	0.42	0.25
Bed density, ρ_B [g/cm^3]	0.70	0.63
Adsorption bed	Breakthrough and VSA	PSA
Length, L [cm]	100	100
Inside radius, R_{Bi} [cm]	1.72	1.1
Outside radius, R_{Bo} [cm]	1.987	1.275
Heat capacity of column, C_{pw} [cal/g·K]	0.12	0.12
Density of column, ρ_w [g/cm^3]	7.83	7.83
Internal heat transfer coefficient, h_i [cal/cm^2·K·sec]	9.2E-4	9.2E-4
External heat transfer coefficient, h_o [cal/ cm^2·K·sec]	3.4E-4	3.4E-4

Zeolite 13X (Zeochem Co.) and CMS (Takeda Chem., 3A) were used as adsorbents for the breakthrough, VSA and PSA experiments. Prior to the experimental runs, the zeolite 13X were regenerated at 613 K overnight and the CMS at 423 K. The ternary mixture (N_2/O_2/Ar; 78:21:1 vol.%, DaeSung Industrial Gas Co.) was used as a feed gas for the breakthrough and VSA experiments while the binary (O_2/Ar; 95:5 vol.%) mixture was used for the PSA experiments. More detailed properties of the adsorbents and the adsorption bed are presented in Table 1.

4. Process Description

The cyclic sequences for the five-step VSA and six-step PSA were illustrated in Table 2. The VSA for air separation adopted the Skarstrom-cycle with pressure equalization step. And this process consisted of conventional VSA steps such as pressurization (PR), adsorption (AD), blowdown (BD), vacuum (VU), PPE (Pressurizing pressure equalization), and DPE (Depressurizing pressure equalization) steps.

In the oxygen purification process, the modified six-step PSA process was operated to obtain the high purity oxygen of 99.8+%. The flow direction of all the steps except BD step was co-current. The idle time was applied to keep the cyclic symmetry. Especially, the two-stage (high to medium pressure—BD1, and medium to ambient pressure—BD2) BD steps were introduced in order to control the purity and recovery of the PSA process. The effluent from the first blowdown step followed after the AD step was used as a purge gas for the other bed. Then, the second blowdown step produced an oxygen product.

5. Results and Discussion

The adsorption isotherms of N_2, O_2 and Ar on zeolite 13X and CMS were measured by a volumetric method. The adsorption isotherms on CMS were measured up to the high pressure ranges for the PSA process while those on zeolite 13X were measured at the low pressure regions for the VSA process. Zeolite 13X showed noticeable equilibrium selectivity between N_2 and O_2 throughout the experimental pressure ranges. However, there was no distinguishable difference in equilibrium amount among O_2, Ar, and N_2 at up to 5 atm.

As can be seen in Fig. 1(a), the kinetic selectivity among three adsorbates on zeolite 13X was not prominent. Moreover, the diffusion time constants did not show any dependence on concentration. However, as shown in Figs. 1(b) to (d), the kinetic selectivity in the Ar/O_2 and N_2/O_2 systems on CMS was quite noticeable all over the experimental pressure ranges. Therefore, it is expected that Ar and N_2 removal from the O_2 rich gas can be applied successfully to the CMS bed. In

Table 2. Cyclic sequences and step times of VSA and PSA processes.

VSA for air separation (↑: Cocurrent flow, ↓: Countercurrent flow)						
BED I	PR↑	AD↑	DPE↑	Vacuum↓		PPE↓
BED II	Vacuum ↑		PPE↓	PR↑	AD↑	DPE↑
PSA for oxygen purification (↑: Cocurrent flow, ↓: Countercurrent flow)						
BED I	PR ↑	AD ↑	BD1 ↓	BD2 ↓ (O_2 produced)	ID	PU ↑
BED II	BD2 ↓	ID	PU ↑	PR ↑	AD ↑	BD1 ↓

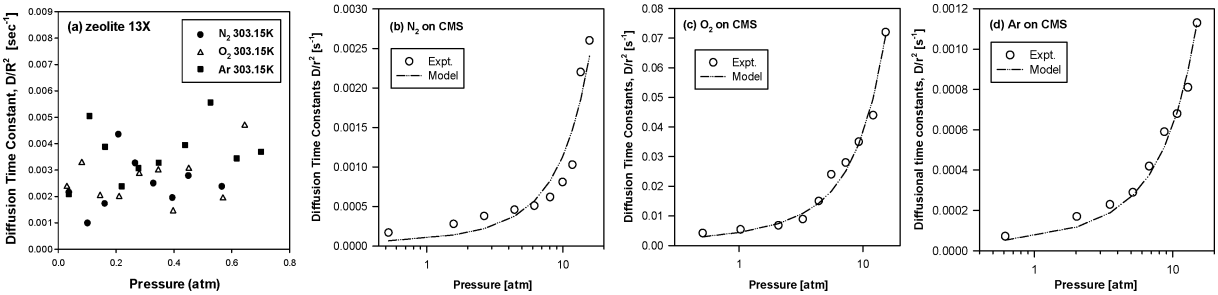

Figure 1. Effect of adsorption pressure on the variation of diffusion time constants of N_2, O_2, Ar on (a) zeolite 13X and (b) N_2, (c) O_2, (d) Ar on CMS.

addition, the modified structural diffusion model fitted well with the experimental concentration dependency of diffusion time constants.

5.1. Breakthrough Experiments

The breakthrough curves for N_2, O_2, and Ar on the CMS bed are shown in Fig. 2(a). As an initial condition, He, non-adsorptive, was used to pressurize the bed to adsorption pressure. As shown in this figure, Ar was the first breakthrough component at about 110 sec, followed by N_2 at a very close interval of 5–10 sec. In particular, the breakthrough curve for N_2 was very steep and showed little tailing while that of Ar was relatively broad and showed a small excursion. At the N_2 plateau, N_2 concentration increased slightly with time until the breakthrough of Ar had finished. Then, it began to decrease with a tail at the beginning of the breakthrough of O_2. The breakthrough of O_2 appeared at about 250 sec, showing a weak roll-up phenomenon. It implies that N_2 and Ar can be removed at an adsorption step and O_2 with high purity can be produced at a blowdown step in the CMS PSA.

Figure 2(b) shows the breakthrough curves of air at the zeolite 13X bed saturated by O_2. The breakthrough of Ar occurred after 200 sec with the sharp roll-up due to the strong adsorption of N_2. And the breakthrough of N_2 followed after the short interval of about 10 sec. The velocity of the N_2 mass transfer zone (MTZ) was fairly fast because the concentration of N_2 in the feed was relatively high regardless of its high adsorption capacity.

The roll-up phenomenon of zeolite 13X bed occurred when the weakly adsorbed components, Ar, lost their adsorption sites due to the competitive equilibrium adsorption of more strongly adsorbed components. However, although the partial pressure of N_2 in the feed is much higher than that of the others, the roll-up phenomena in the CMS bed mainly stemmed from the great kinetic difference between O_2 and N_2/Ar because the equilibrium selectivity of O_2, N_2 and Ar on CMS is negligible.

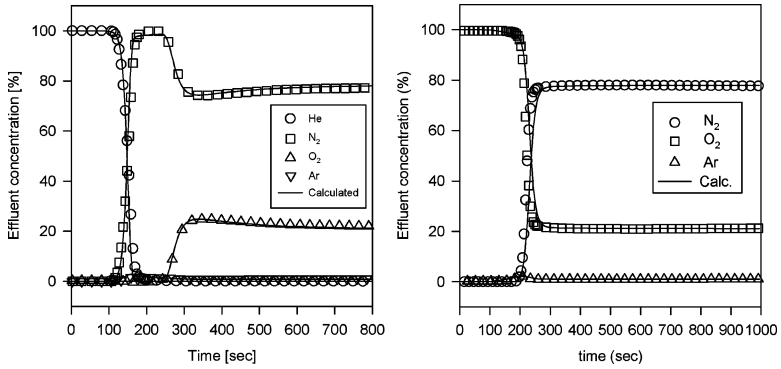

Figure 2. Breakthrough curves of N_2, O_2, and Ar on (a) CMS bed at 5 atm and 4 LSTP/min and on (b) zeolite 13X bed at 1.5 atm and 2 LSTP/min.

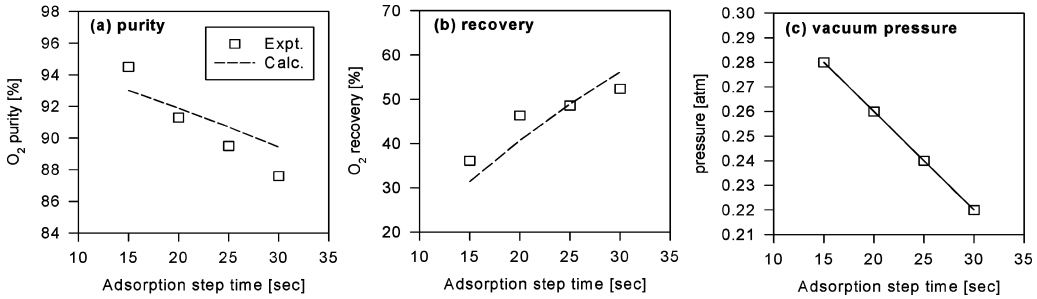

Figure 3. Variation of (a) O_2 purity, (b) O_2 recovery, and (c) vacuum pressure of VSA process at various AD step times. (1.8 atm adsorption pressure and 1.3 LSTP/min feed flow rate conditions.)

5.2. *VSA Process for Air Separation*

The effects of AD step time on O_2 purity and recovery are shown in Fig. 3 and Table 3. In Fig. 3(a), purity decreased as the AD step times increased. This is because the increased AD step time led to a breakthrough of N_2 toward the bed end. Purity decreased somewhat broadly because the VU step time increased simultaneously with the AD step time. However, the lower regeneration pressure by the increased VU step time in Fig. 3(c) could not offset the improvement in purity. In Fig. 3(b), recovery increased almost linearly with the extension of AD step times because the prolonged AD step time caused the increment of the net product amount. As a result, the oxygen of 90+% oxygen can be produced with the recovery of 50% in the zeolite 13X VSA.

The N_2 mole fraction at the end of AD step was kept constant for about 15 sec regardless of the propagation of N_2 MTZ. However, after 15 sec, the bed end was gradually contaminated because the N_2 MTZ propagated noticeably to the bed end. The VU step time was also extended with an increase in AD step time to maintain the cyclic symmetry. However, the extended VU step time could not reduce the remaining N_2 amount at the end of the VU step. This is because the increment of remaining N_2 amount at the AD step exceeded the increased desorption amount at the VU step in the case of simultaneous extension of the AD and VU step times.

Table 3. Steady state O_2 purity and recovery of VSA process at 5 atm and 4 LSTP/min.

Adsorption step time [sec]		O_2 purity [%]	O_2 recovery [%]
25	Expt.	93.85	56.80
	Calc.	94.05	50.60
30	Expt.	93.55	64.07
	Calc.	91.97	58.85
35	Expt.	91.49	70.71
	Calc.	89.77	65.82
40	Expt.	87.02	75.56
	Calc.	87.49	71.71

5.3. *PSA Process of Oxygen Purification*

The performance of the PSA process using a binary mixture is presented in Table 4. The purification process produced high purity oxygen of 99.8+% with high recovery and productivity because O_2 was obtained mainly from the adsorbed phase after removing Ar from the gas phase. The result implies that the oxygen product from the VSA process can be successfully purified by the PSA process. In addition, the modified LDF model with a concentration-dependent diffusivity showed a good prediction in the experimental results at a steady-state.

Figure 4 shows the MTZ and velocity profiles at the end of each step along the bed. In Fig. 4(a), the O_2 concentration at the end of the PR step showed a favorable decrease near the bed end because Ar in the gas phase was concentrated at the bed end by O_2 adsorption. At the end of the AD step in Fig. 4(b), O_2 concentration

Table 4. Steady state O_2 purity, recovery and productivity of PSA process at 5 atm and 4 LSTP/min.

	O_2 purity [%]	O_2 recovery [%]	Productivity [mmol/g·sec]
Expt.	9.87	56.90	5.97×10^{-3}
Calc.	99.86	58.23	6.10×10^{-3}

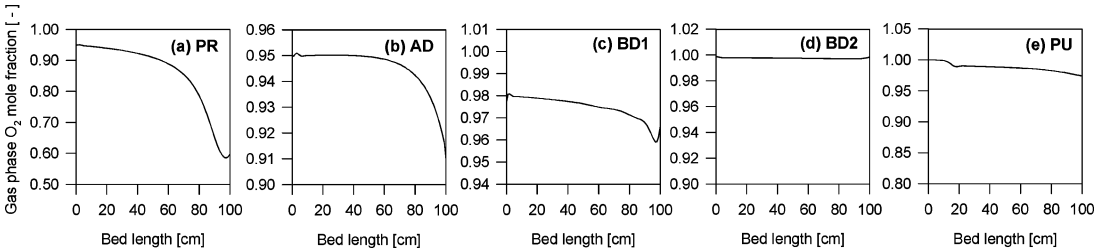

Figure 4. O_2 concentration profiles in the gas phase at each step of PSA process at 5 atm and 4 LSTP/min.

decreased steeply and nearly approached the bed end. The adsorbed phase nearly reached the saturated condition with O_2 at the feed inlet boundary and a certain amount of Ar, which could not diffuse into the CMS, was concentrated in the vicinity of the bed end. At the end of the BD1 step in Fig. 4(c), the high purity O_2 was purged to the other bed. However, a certain amount of desorbed Ar remained in the gas phase. Moreover, the O_2 concentration profiles were a concave shape observed in the bed end. Because Ar was concentrated at the bed end in the previous step, the adsorbed Ar at this part of the bed desorbed very slowly. At the end of the BD2 step in Fig. 4(d), the whole bed was virtually kept clean with high purity O_2 of over 99.5% because most of the impurities in the gas phase were vented in the previous step. At the end of the PU step shown in Fig. 4(e), the feed inlet was kept clean with high purity O_2 received from the other bed. However, as the adsorption of O_2 proceeded, the O_2 mole fraction in the gas phase decreased gradually.

Acknowledgment

The financial support of the Carbon Dioxide Reduction and Sequestration R & D Center (C002-0103-001-1-0-0) is gratefully acknowledged.

References

Bae, Y. and C.-H. Lee, "Sorption Kinetics of Eight Gases on a Carbon Molecular Sieve at Elevated Pressure," *Carbon*, **43**, 95–107 (2005).

Do, D.D., "A Model for Surface Diffusion of Ethane and Propane in Activated Carbon," *Chem. Eng. Sci.,* **51**, 4145–4154 (1996).

Hayashi, S., M. Kawai, and T. Kaneko, "Dynamics of High Purity Oxygen PSA," *Gas Sep. & Purif.,* **20**, 19–23 (1996).

Jee, J.-G., H. Park, S. Haam, and C.-H. Lee, "Effects of Nonisobaric and Isobaric Steps on O_2 Pressure Swing Adsorption for an Aerator," *Ind. Eng. Chem. Res*., **41**, 4383–4392 (2002).

Kim, M.B., J.H. Moon, C.H. Lee, M. Oh, and W. Cho, "Effect of Heat Transfer on the Transient Dynamics of TSA Process," *Korean J. Chem. Eng.*, **21**, (2004).

Yang, R.T., *Gas Separation by Adsorption Processes*, Butterworths, Boston, 1987.